Supporting information

Development of Au and 1D Hydroxyapatite Nanohybrids Supported on 2D Boron Nitride Sheets as Highly Efficient Catalysts for Dehydrogenating Glycerol to Lactic Acid

G. Bharath*, K. Rambabu, Abdul Hai, Hanifa Taher, Fawzi Banat*

Department of Chemical Engineering, Khalifa University of Science and Technology, P.O. Box 127788, Abu Dhabi, United Arab Emirates.

Corresponding Authors; Prof.Fawzi Banat, E-Mail: fawzi.banat@ku.ac.ae

Dr.G. Bharath E-Mail: sribharath7@gmail.com

bharath.govindan@ku.ac.ae

Number of pages: 6

Number of figures: 5

Number of tables: 1

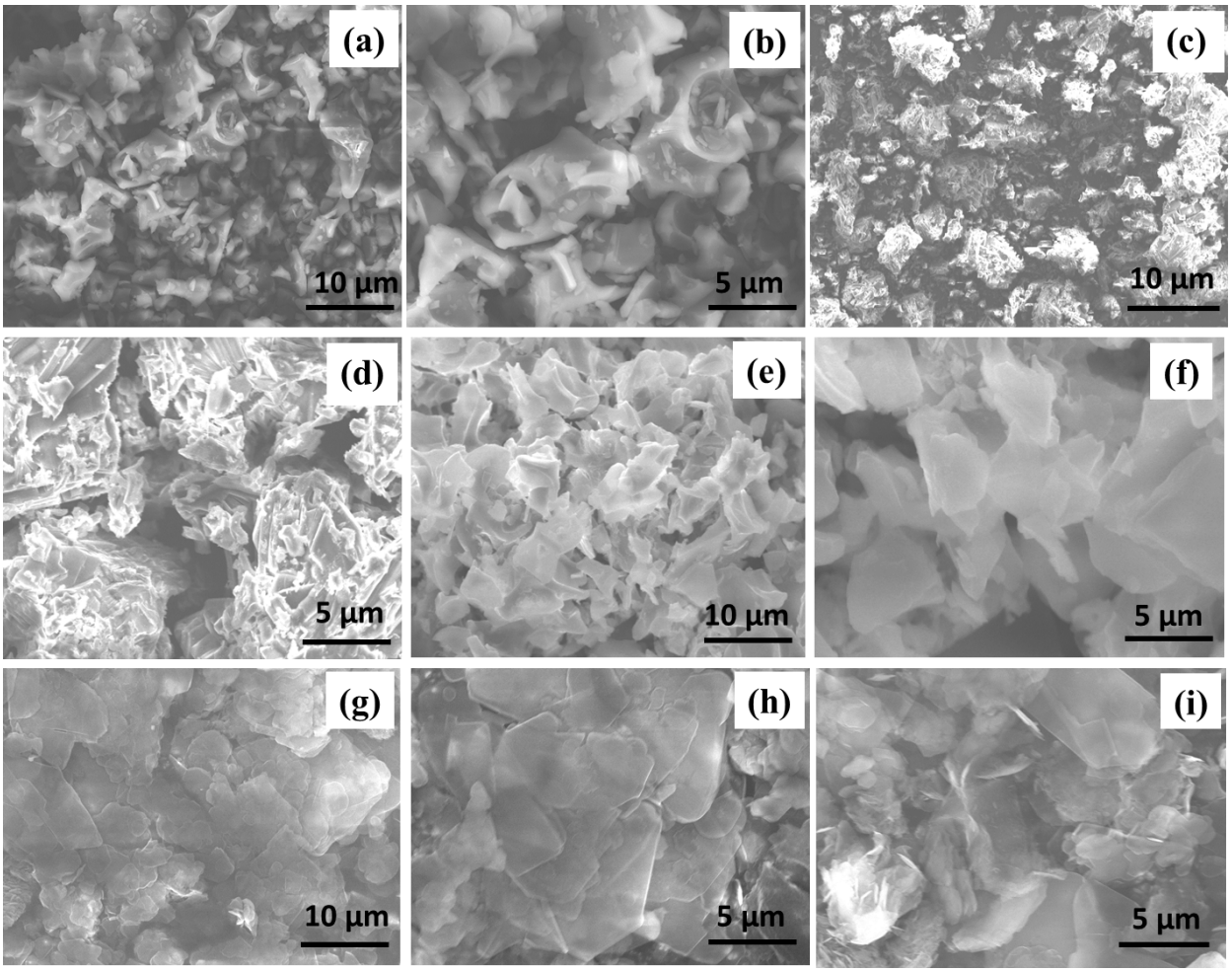

Figure S1. (a) and (b) SEM images of as-prepared BN using without template via tubular furnace at 900 °C for 4 h, in N_2 atmosphere, (c) and (d) SEM images of pre-heated BN/banana stem sample at 70 °C overnight, (e) and (f) SEM image of calcined BN via tubular furnace at 450 °C for 2 h, in air atmosphere, (g) and (h) SEM image of as-prepared BN via tubular furnace at 900 °C for 4 h, in N_2 atmosphere, and (i) SEM image of individual BN sheets after dispersion in ethanol under sonication for 30 min.

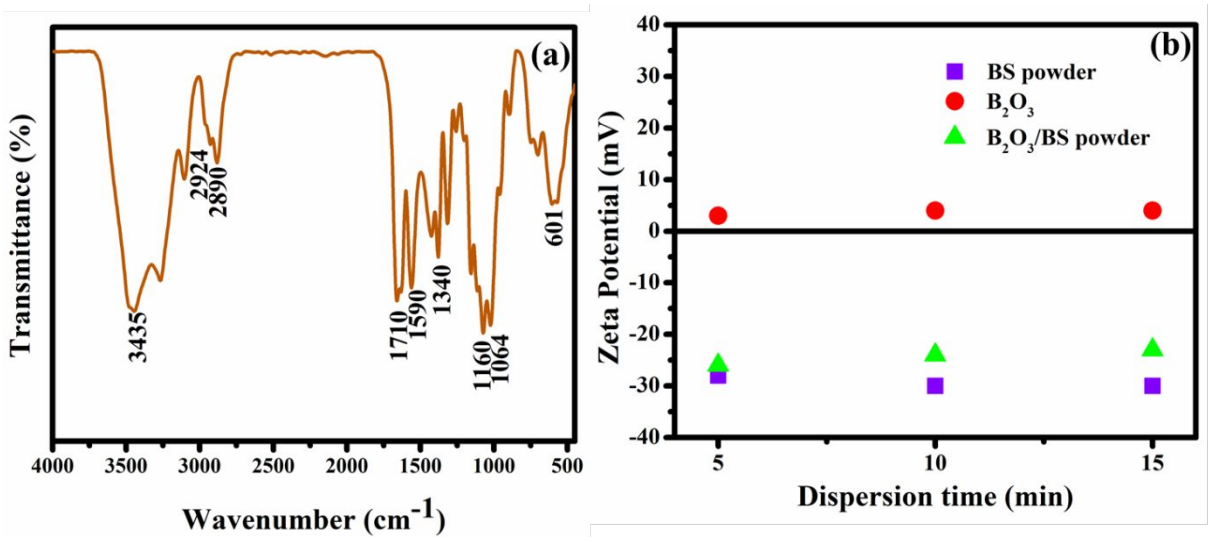

Figure S2. (a) FT-IR spectra of BS powder and (b) Zeta potential analysis of the BS powder, B_2O_3, B_2O_3/BS powder in ethanol as a function of dispersion time under mild sonication

The functional groups of the BS powder were determined by FT-IR spectra as shown in Fig.S1(a). A broad band at 3435 cm^{-1} corresponded to the stretching vibration of hydrogen bond in the OH groups of cellulose. Two bands observed at 2924, and 2890 cm^{-1} were associated to the –CH asymmetric and symmetric stretching vibrations of methylene hydrogen, respectively. The intense bands at 1710, 1590, and 1340 cm^{-1} were associated to the vibrations of C=O bond of lignin or hemicelluloses, C–O stretching of alcohol and sulfoxides respectively. High intense bands at 1160 and 1064 cm^{-1} could be ascribed to carbohydrates or polysaccharide-like substances and υ(C–O–C) asymmetrical stretching, respectively. The high intense band at 601 cm^{-1} was associated to the bending vibration of C-H out of plane. The existence of the main functional groups of OH, =CH, C=O and $–NH_2$ groups in the BS powder were responsible for the adsorption of B_2O_3.

Further, zeta potential analysis was used to determine the interaction between BS powder and B_2O_3. Zeta potential analysis of the BS powder, B_2O_3 and B_2O_3/BS powder were performed after thorough sonication of the samples dispersed in ethanol. Concentration of additive was 0.1 mg/ml in each case, and it was added in the nanosuspension. Furthermore, the time-dependent zeta potential measurements were repeated at least three times to assess the colloidal stability and surface charges of the solutions. Fig.S1(b) shows the zeta potential of BS powder, B_2O_3 and B_2O_3/BS powder at different times of 5, 10 and 15 min under sonication. The BS powder displayed a high, negative zeta potential of -28 mV at 5 min and then reached a maximum absolute zeta

potential value of -31 mV at 15 min. This result indicated the complete dispersion of BS powder in ethanol at 15 min under sonication which resulted in its maximum and stable zeta potential value. The zeta potential of B_2O_3 was slightly positive with maximum absolute value of 4 mV at 15 min. After mixing of BS powder and B_2O_3, zeta potential of the BS/B_2O_3 composite became significantly less (compared to B_2O_3) to a negative value of -24 mV at 15 min. This confirmed the successful adsorption of positively charged boron on the surfaces of negatively charged BS powder via electrostatic interactions. Significance of this studies revealed that the BS powder used as green template to produce high quality BN NSs.

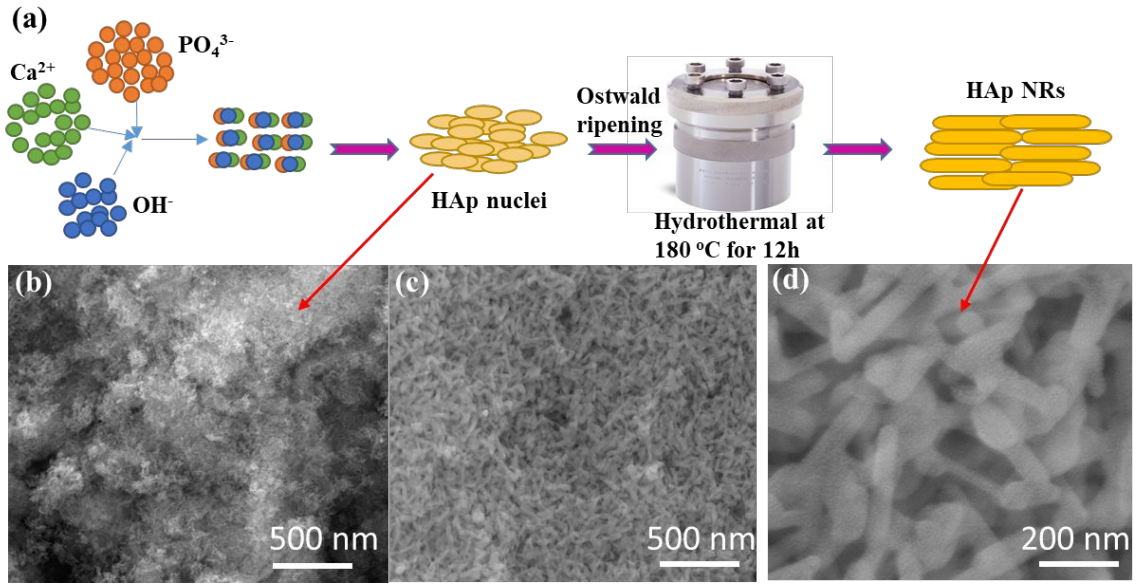

Figure S3. (a) Schematic illustration for the formation of HAp nuclei (HAp_n) and Ostwald ripening growth of HAp via hydrothermal process at 180 °C for 12 h, (b) SEM image of HAp_n, and (c&d) SEM images of HAp NRs.

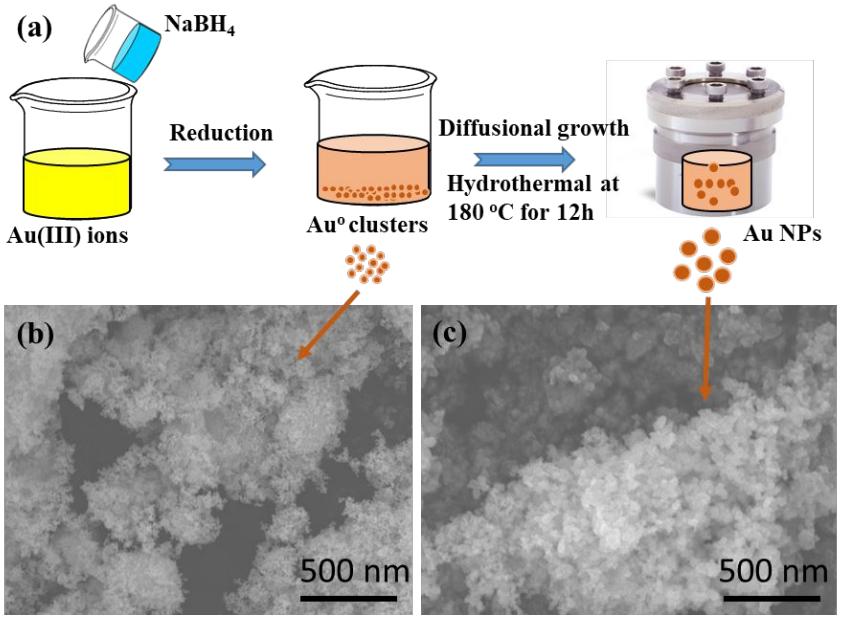

Figure S4. (a) schematic illustration for the formation of Au^{o} clusters during the reduction process and diffusional growth of Au NPs via hydrothermal process at 180 ^{o}C for 12 h, (b) SEM image of Au^{o} clusters, and (c) SEM image of Au NPs.

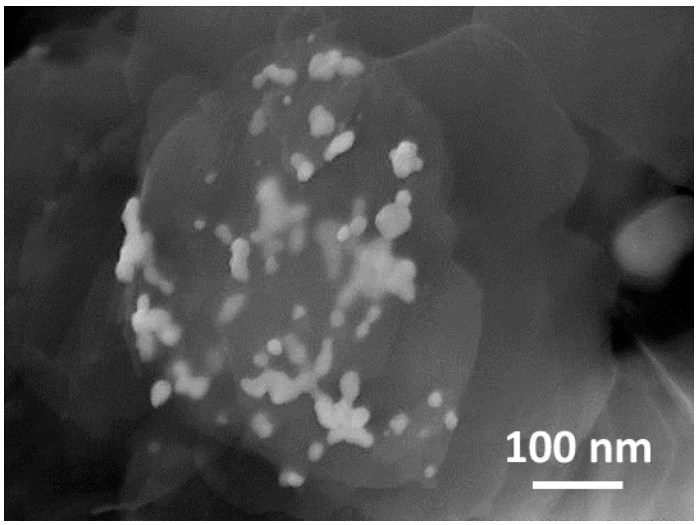

Figure S5. SEM image of Au/BN nanocomposite

Table S1. Conversion of glycerol into lactic acid, and other common intermediates, using various catalysts of BN NSs, c-BN NPs, control, Au/BN, HAp/BN, and Au/BN/HAp

Catalyst	$Con._{Gly}$ (%)	$Y_{.LA}$ (%)	Selectivity in the conversion of glycerol (%)				
			LA	GA	1,2 Pr	Py	Others
BN NSs	66	48	72	6	7	9	6
c-BN NPs	43	36	64	6	2	6	7
Control	30	17	56	10	16	13	7
Au/BN	75	55	74	5	7	5	9
HAp/BN	80	60	75	4	6	12	3
Au/BN/HAp	95	85	90	2	3	3	2

Note: Reaction conditions; NaOH to glycerol molar ratio = 1:1, reaction temperature = 100 ^{o}C, reaction time=60 min, catalyst dosage = 20 mg, atmosphere = Air.